12th International Symposium on Turbulence and Shear Flow Phenomena (TSFP12)
Osaka, Japan (Online), July 19-22, 2022

TURBULENT BOUNDARY-LAYER RESPONSE TO ACTIVE ROUGHNESS

Aditya Ramani
Department of Mechanical Engineering
The University of Melbourne
Parkville, Victoria 3010, Australia
ramania@student.unimelb.edu.au

Jason P. Monty
Department of Mechanical Engineering
The University of Melbourne
Parkville, Victoria 3010, Australia
montyjp@unimelb.edu.au

Nicholas Hutchins
Department of Mechanical Engineering
The University of Melbourne
Parkville, Victoria 3010, Australia
nhu@unimelb.edu.au

ABSTRACT

This experimental study investigates the response of a wall-bounded turbulent flow to an oscillating rough surface. The roughness elements are actuated between a smooth and a roughened state at a single frequency and hot-wire measurements are acquired directly above the oscillating rough wall. The dynamic roughness has a broadband effect on the energy of the flow, increasing the energy beyond that of the static smooth case from the wall to beyond the log region. The phase averaged velocity profiles suggest that, for lower frequencies, the mean flow oscillates between two quasi-steady states: a 'rough' state and a 'smooth' state. These quasi-steady states are separated by a transition state, which is a forward leaning front in phase that marks the departure of the phase average mean from the static limit. As the dimensionless frequency is increased, the transition state is seen to grow as a fraction of the phase cycle, eventually exceeding the half-cycle point where the wall condition changes. At this point, the mean profile is perpetually in transition and the quasi-steady states no longer exist. This behaviour is modelled using an internal boundary layers (IBL) based method. A simple relationship to relate phase to an equivalent spatial location of a step change in roughness is proposed from which the IBL height can be estimated. This is confirmed by comparison with static streamwise heterogeneous data and a good match is seen at the correct phase. The modelled front based on this relationship is seen to match the shape of the front identified from the experiments, and captures the broad changes in the inclination of the front with increasing dimensionless frequency. Thus, a case can be made that turbulent boundary-layers over oscillating roughness can be modelled as growing internal layers.

INTRODUCTION

Wall-bounded turbulent flows commonly occur over many important engineering systems, such as ships, airplanes and turbine blades. The turbulence induced drag reduces the efficiencies of these systems and therefore increases their operating costs. The presence of roughness on the surfaces of these systems, which is often unavoidable in practical applications, increases drag further above smooth wall levels. Predicting this increased drag from the topographical properties of the roughness is a highly sought after goal (Chung *et al.*, 2021). Studies geared towards this goal often assume that the roughness is made up of rigid and invariant elements that are homogeneously distributed. The turbulent boundary layer that develops over such surfaces is said to be in 'equilibrium' with the wall-condition. However, practical roughness can have both spatial and temporal heterogeneity. An example of the former is patchy biofouling on ship hulls while an example of the latter is the soft filamentous biofouling seen on ships (Hartenberger *et al.*, 2020). The consequence of heterogeneity is that the boundary layer is not in equilibrium (i.e. only in the near-wall region is the flow fully-adapted to the local wall conditions). The full-scale and generalised prediction of drag requires studying such surfaces as well.

The case of spatial heterogeneity is often distilled to the problem of streamwise step changes in roughness (either smooth-to-rough, S-R, or rough-to-smooth, R-S). In these cases, the transition of the mean flow downstream of the step is marked by the observation of internal boundary layers (Antonia & Luxton (1971, 1972), Li *et al.*, 2021). In comparison, studies of temporally heterogeneous roughness are rare. While there is some evidence to suggest that oscillating roughness elements increase skin-friction drag beyond a static equivalent surface (Stoodley *et al.*, 1998, Hartenberger *et al.*, 2020), an investigation of the dynamic properties of the roughness in relation to the flow is lacking. The work of Jacobi & McKeon (2011) showed that when a well defined dynamic roughness impulse (sine wave) is imparted to a turbulent boundary layer, the phase-locked effects can be discerned in both the mean and higher-order statistics far downstream of the impulse.

The present study aims to investigate flows developing over a well-defined dynamic roughness which can be actuated between a smooth and a roughened state. The frequency of the roughness is systematically varied and the flow is allowed to develop over the dynamic wall. Flow statistics are acquired directly above the dynamically actuated wall in the developing boundary layer, allowing the effects of the dimensionless outer-scaled frequency on the boundary-layer flow to be investigated.

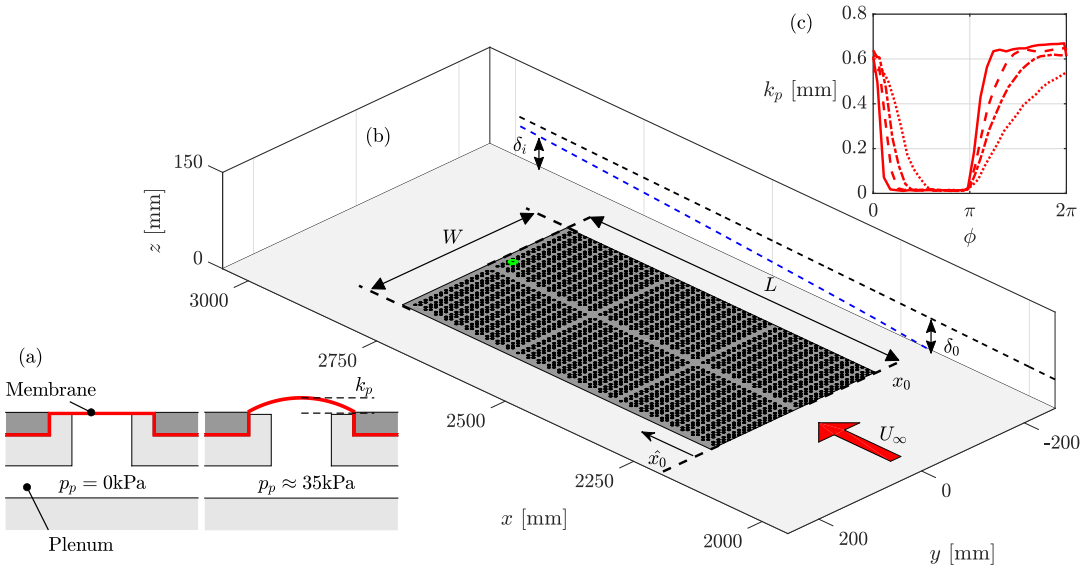

Figure 1: Details of the dynamic roughness experiment: (a) Cross-section of the roughness generation device showing the operation of one element; (b) layout of the device in the wind-tunnel with the flow direction indicated by the arrow and the green dot showing the hot-wire measurements location; (c) mapping of the roughness element height to phase for the frequencies in the study. See Table 1 for the line-types.

EXPERIMENT SETUP

Table 1: Experiment details: All cases are at a free-stream velocity of $U_\infty = 10.03 \pm 0.03$ ms^{-1}. For the active cases, the non-dimensional roughness height, $k_p^+ = k_p U_\tau/\nu$, is scaled with the U_τ for S0 case.

Active Measurements				
Label	f [Hz]	f_δ	k_p^+	Legend
F009	2	0.009	21	
F019	4	0.019	19	
F028	6	0.028	19	
F047	10	0.047	17	

Static Measurements					
Label	p_p [kPa]	U_τ [ms^{-1}]	k_p^+	Re_τ	Legend
S0	0	0.398	—	1180	
R0	35	0.492	23	1480	

An active roughness generation device is designed for this study, which generates roughness elements by inflating a synthetic latex membrane through a perforated metal plate. The peak height of the roughness elements, k_p, can be varied by adjusting the input pressure, p_p (gauge), to the plenum. This arrangement is illustrated in Figure 1(a). The device has an area of 0.66m $\times$ 0.338m. In the present study, the pressure is cycled between $p_p = 0$kPa and a maximum of $p_p = 35$kPa to produce a oscillating rough surface. Compressed air, regulated to $p_p = 35$kPa with a Festo MS6-LR-1/2-D5-AS manual pressure regulator, is supplied to a common reservoir (Festo CRVZS-10). The plenums are connected to the reservoir with rubber hoses ($\varnothing$= 4mm). The cycling is achieved through miniature solenoid valves (Emerson ASCO 411L3305HV) that are connected in line with the hoses and located directly underneath the plenums. Pairs of adjacent plenums are controlled by the same valve. Custom designed circuit boards and software are used to control and switch the valves remotely. For the oscillating roughness, the valves are switched simultaneously with a square wave input thus producing a oscillating rough surface.

The roughness device is installed in an open-return type wind-tunnel at the Walter Basset Aerodynamics Laboratory at the University of Melbourne. The working section of the tunnel is 6.7m long with a cross-section area of 0.94m $\times$ 0.375m. The boundary layer is tripped to turbulent at the inlet of the tunnel by a strip of P40 grit sandpaper (see Marusic & Perry, 1995 for further details on the facility). The upstream, side and downstream portions of the tunnel floor surrounding the device are made up of smooth MDF panels. Flow statistics are acquired using hot-wire anemometry. The sensor is located at a streamwise distance of $x \approx 2.8$m from the inlet of the tunnel, which corresponds to a fetch of $\hat{x} \approx 0.63$m over the device. See Figure 1(b) for a schematic of the device setup and hot-wire measurement location. A modified Dantec 55P05 boundary-layer probe with a 5µm diameter Wollaston wire is used with a Melbourne University Constant Temperature Anemometer (MUCTA). The sensing element of the hot-wire is etched to a length of 1mm (corresponding to $l^+ \approx 30$, where the $+$ superscript denotes viscous scaling, i.e. $l^+ = lU_\tau/\nu$, where U_τ is the friction velocity and is defined as $U_\tau = \sqrt{\tau_w/\rho}$, and ν is the kinematic viscosity) such that $l/d \approx 200$ in order to minimise end-conduction effects (Ligrani & Bradshaw, 1987). Sensor calibration is performed prior to and after each wall-normal traverse and drift is corrected with in-situ measurements in the free-stream following the method of Talluru *et al.* (2014). The hot-wire sensor is sampled simultaneously with the square-wave input to the valves to allow for phase averaging. Sampling frequency is set to 48kHz which gives a dimensionless sampling frequency of $f^+ \approx 4.5$. Sampling time is based on

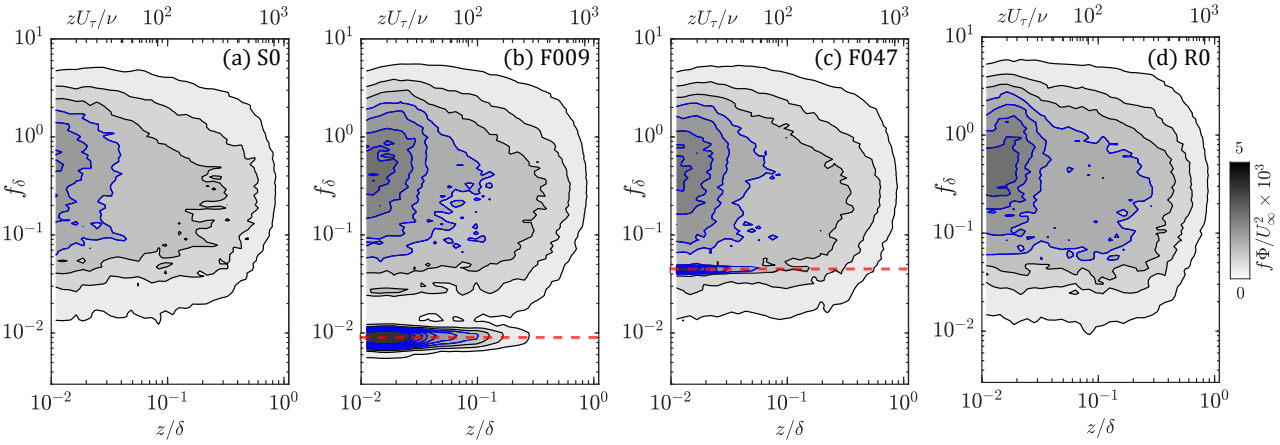

Figure 2: Pre-multiplied energy spectrograms of the streamwise velocity ($f\Phi_{uu}$) for cases: (a) Static smooth (S0), (b) active F009, (b) active F047 and (d) static rough (R0). Contours marked in blue are regions where $f\Phi_{uu}/U_\infty^2 \times 10^3 \geq 1.6$. The wall-normal height with inner-scaling shown on the top is with the U_τ of the smooth (S0) case. The red dashed line indicates the dimensionless actuation frequency for the active cases.

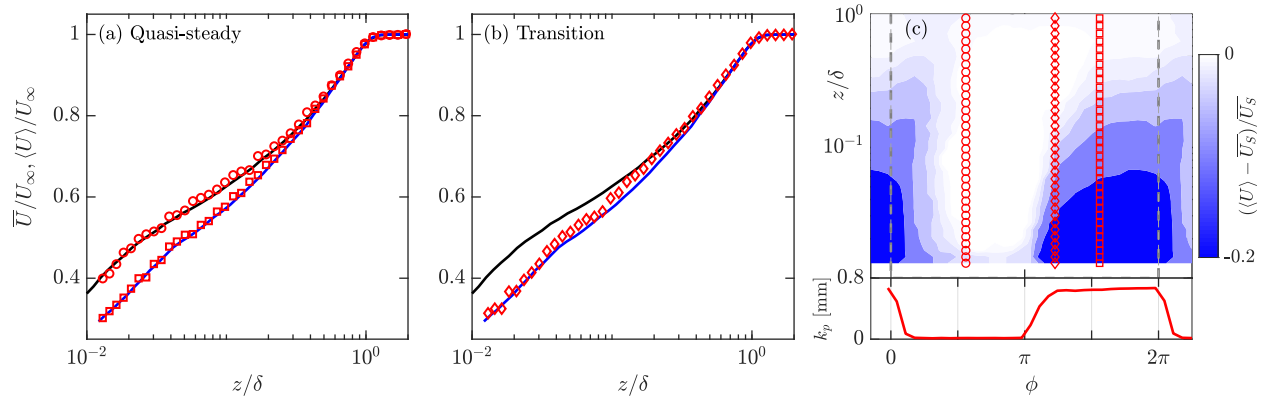

Figure 3: Phase averaged mean velocity profiles, $\langle U \rangle$, for the F009 case showing (a) Quasi steady behaviour at $\phi = \pi/2$ (○) and $\phi = 3\pi/2$ (□) and (b) transition behaviour at $\phi = 1.2\pi$ (◇). The S0 (—) and R0 (—) profiles are also shown. Fluctuation of the phase average from the smooth (S0) limit $(\langle U \rangle - \overline{U_S})/\overline{U_S}$ is shown in (c) along with the roughness element height, k_p as a function of phase. The phase positions from (a) and (b) are shown with matching symbols.

the boundary layer turnover time such that $TU_\infty/\delta > 20,000$. Here, U_∞ is the free-stream velocity and δ is the height where the mean velocity recovers to 98% of U_∞. The free-stream velocity for all cases is $U_\infty = 10.03 \pm 0.03 \text{ms}^{-1}$.

Statistics are acquired for both the active and static operation of the device in a zero pressure gradient (ZPG) turbulent boundary layer. For the active operation, the frequencies studied are $f \in [2,4,6,10]$ Hz, which corresponds to a dimensionless outer-scaled frequency of $f_\delta = f\delta/U_\infty \approx 0.009$ to 0.047 ($f^+ \approx (1.8 \text{ to } 9.5) \times 10^{-4}$). The roughness element peak height, k_p, is measured as the height of the centre of the roughness element from its unactuated position. A Keyence LK-031 laser triangulation sensor is positioned over the centre of an element and the height is sampled simultaneously with the square-wave actuation signal. Samples are obtained over multiple elements to check for consistency. For each of the frequencies in this study, k_p is mapped as a function of phase ($\phi \in [0, 2\pi]$) as shown in Figure 1(c). For static operation, measurements are acquired at $p_p = 0$kPa (i.e. 'smooth', case label S0) and $p_p \approx 35$kPa (i.e. 'rough', case label R0), corresponding to the limits of the active oscillating case. The details of the dynamic and static cases are listed in Table 1 along with the legend for their depiction throughout this paper. For the static cases, the friction velocity, U_τ is estimated using a modified-Clauser method in the log region ($100 \leq z^+ \leq 0.15\delta^+$). The roughness function varies from $\Delta U^+ \approx 0.9$ for the S0 case to $\Delta U^+ \approx 5.9$ for rough R0 case (the latter corresponding to a $k_s^+ \approx 45$ assuming fully rough conditions). Thus, switching between the S0 and R0 cases corresponds to a $Re_\tau = U_\tau\delta/\nu$ variation between $1180 - 1480$ $U_\infty = 10 \text{ms}^{-1}$.

RESULTS

In Figure 2(b), contours of the pre-multiplied energy spectra, of the F009 case are shown. This spectra is the energy of the fluctuations of the streamwise velocity about the time-averaged mean. The effect of the dynamic roughness is seen as a band of energy in the flow centered on f_δ (marked by the red-dashed line). The energy band is seen to extend into the boundary-layer to a height of $z/\delta \approx 0.3$ (or $z/k_p \approx 20$). This is beyond the typical upper limit of the logarithmic region ($z/\delta \approx 0.15$ or $z^+ \approx 180$). As the actuation frequency encroaches more on the energetic scales of turbulence, as shown in Figure 2(c) for case F047, the band is obscured by the energy of the flow, and the wall-normal extent into the bound-

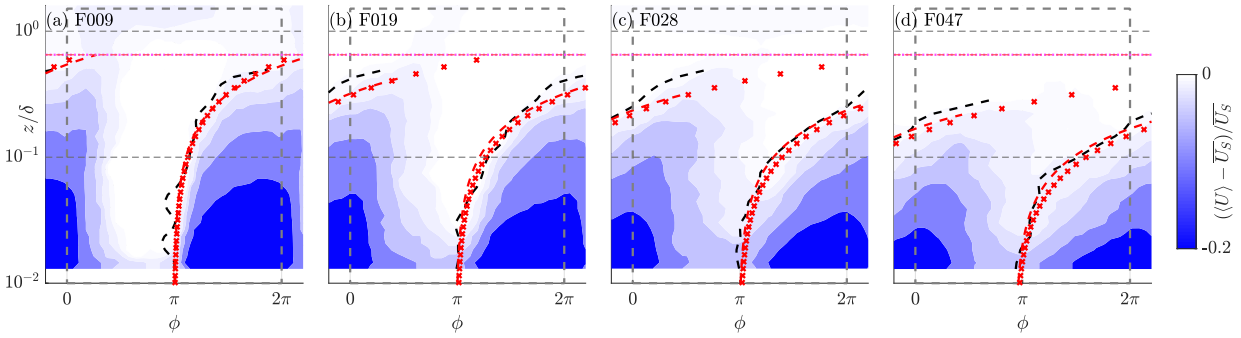

Figure 4: Fractional fluctuation of the phase averaged velocity about the smooth limit, $(\langle U\rangle - \overline{U_S})/\overline{U_S}$, with f_δ increasing from 0.009 to 0.047 in plots (a) to (d). The (- -) lines mark the front where the mean velocity departs from the 'smooth' limit, i.e. the minimum of $|\langle U\rangle - \overline{U_S}|$. Also shown is the IBL height, δ_i, modelled with Equation (3) (- - -) and Equation (4) (×). The (···) line is at $z/\delta = 0.65$ indicating the upper limit to which the IBL is expected to grow for the static rough surface based on Equation 1.

ary layer is seen to diminish. The actuation frequencies in this study, except for the F047 case (10Hz), are low in comparison to the largest structures in the flow, which can exceed 20δ (Hutchins & Marusic, 2007) and have a frequency of $U_\infty/20\delta \approx 11$Hz. In Figure 2(a) and (d), the energy spectra of the S0 and R0 cases are shown respectively. As shown by the blue contours, which correspond to $f\Phi_{uu}/U_\infty^2 \times 10^3 > 1.6$, outside the band corresponding to the actuation frequency, the broadband energy of the active cases appear to be elevated above the static smooth case S0 but lower than that of the static rough case R0.

To understand this, we look at the phase averaged mean velocity ($\langle U\rangle$), which is the mean velocity at the corresponding phase of the dynamic roughness at the wall. This is shown in Figure 3(a, b) for the lowest frequency case (F009) along with the mean profiles for the S0 and R0 cases. At $\phi \approx \pi/2$ (open circles) and $\phi \approx 3\pi/2$ (open squares), the phase averaged profile for case F009 matches the S0 and R0 cases respectively, as shown in Figure 3(a). However, at $\phi \approx 1.2\pi$ (open diamonds), the phase averaged profile lies in a transition state, matching the static rough profile close to the wall and transitioning to the smooth curve further away from the wall, as shown in Figure 3(b). In Figure 3(c), contours of the fractional fluctuation of the phase averaged mean velocity about the S0 case, $(\langle U\rangle - \overline{U_S})/\overline{U_S}$, are shown for the F009 case. Here $\overline{U_S}$ is the time-averaged mean for the S0 case. The three phases represented in Figure 3(a, b) are shown with matched symbols, along with the mapping of the roughness element height to phase. Together, these two figures suggest that for low dimensionless frequencies the mean velocity of the flow oscillates between two quasi-steady states: a 'smooth' state (where $\langle U\rangle \approx \overline{U_S}$) and a 'rough' state (where, $\langle U\rangle < \overline{U_S}$). These two states are separated by a transition state where the profile conforms to the wall condition closer to the wall, but transitions to the previous state at some distance away from the wall.

Figure 4 (a) to (d) show similar plots of the fractional fluctuations for all four tested dimensionless frequencies. The transition front from the smooth response to the rough response can be demarcated as the point where the phase average ($\langle U\rangle$) departs from the smooth limit ($\overline{U_S}$) (identified as the minimum of $\left|\langle U\rangle - \overline{U_S}\right|$). The fronts are shown by the black dashed lines in Figure 4. As f_δ is increased from 0.009 to 0.047, the front becomes more forward inclined and the transition state occupies a larger fraction of each cycle (thus the quasi-steady behaviour diminishes). Assuming that the internal layer growth rate is described by a power-law expression, as suggested by Li *et al.* (2021) and is given as:

$$\delta_i/\delta = A_0(\hat{x}/\delta)^\alpha \tag{1}$$

where $A_0 = 0.094$ and $\alpha = 0.75$, for the fetch from the leading edge of the actuated surface to the measurement location, $\hat{x} = 0.63$m, we might expect that the maximum wall-normal extent for the internal layer in the quasi-steady limit would grow to $z/\delta \approx 0.65$. For the F009 case, the front is seen to reach this limit within the half-cycle (i.e. before the roughness changes at the wall), therefore reaching the quasi-steady state where the measured flow conforms to the R0 case. However, for the F019 case and beyond, the front has failed to reach $z/\delta = 0.65$ even at $\phi = 2\pi$, where the wall condition changes. Therefore, at higher dimensionless frequencies, the quasi-steady state is not reached and the flow remains perpetually in a state of transition. Together, these results suggest that the response of the flow to oscillating roughness can be modelled as the growth of internal boundary layers. This hypothesis forms the basis for the modelling approaches discussed in the next section.

MODELLING THE RESPONSE OF THE BOUNDARY LAYER

Let us consider a frame of reference that is advecting with the flow over the actuating surface, as depicted in Figure 5. The flow is developing over a smooth wall when at ϕ_{trig}, the wall condition is triggered to rough. The flow now develops over a rough wall and flows past the hot-wire sensor at some later phase ϕ_{obs}. The effective fetch, $\hat{x}_e$ that is available for the IBL growth would depend on where on the active surface the observed flow (at ϕ_{obs}) encounters the step change in roughness, which will change as a function of $\phi_{obs} - \phi_{trig}$. This scenario is schematically illustrated in Figure 5. For observations just after ϕ_{trig}, shown in Figure 5(a), the flow that is measured will have experienced the temporal step change to roughness at an effective location that is just upstream of the measurement plane. Thus only the near-wall region will be affected by the new wall condition. At a later ϕ_{obs}, the flow that is measured will have encountered the temporal step change further upstream, leading to an IBL that has developed further away from the wall, which is shown in Figure 5(b). And finally,

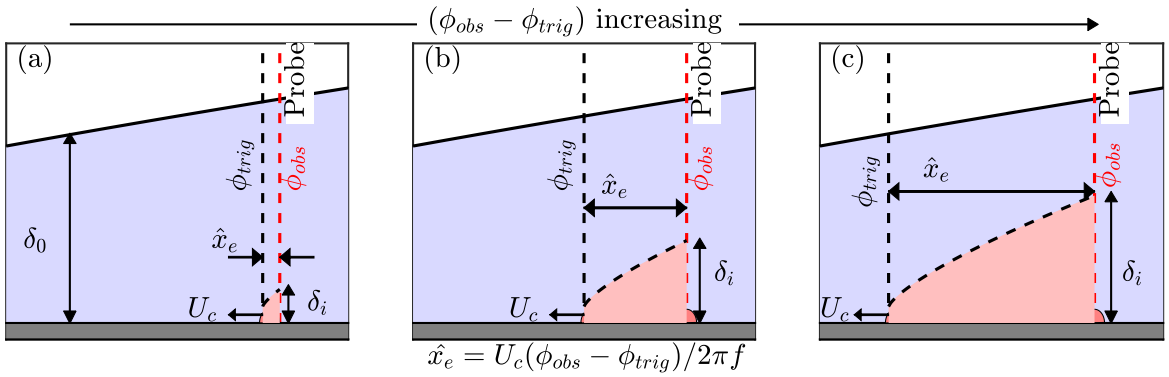

Figure 5: Schematic of the model for IBL growth based on the effective fetch, $\hat{x}_e$, that the flow sees: the flow encounters the step change at ϕ_{trig}, and flows over the new wall condition past the hot-wire probe at ϕ_{obs}, where it is measured. The effective position, $\hat{x}_e$ at which the flow would have encountered the step change advects upstream as ϕ_{obs} increases from (a) to (c), with some velocity U_c. The flow direction is from left to right.

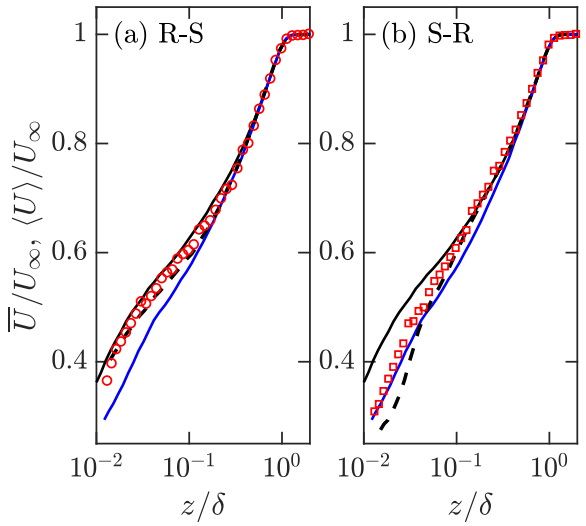

Figure 6: Mean velocity profiles for static step change in roughness (- - -) and the phase averaged profiles of the active F009 case at matched phases based on Equation 2: (a) Static rough-to-smooth case at $\hat{x}/\delta \approx 2.1$ and active case at $\phi \approx 0.22\pi$ (○) and (b) Static smooth-to-rough case at $\hat{x}/\delta \approx 2.1$ and the active case at $\phi = 1.22\pi$ (□). The S0 (—) and R0 (—) profiles are also shown.

at an even later position in phase, the measured flow would have developed over the entire fetch of the installed surface, as shown in Figure 5(*c*). Therefore, an effective fetch, $\hat{x}_e$, can be estimated for each ϕ_{obs} as:

$$\hat{x}_e = U_c(\phi_{obs} - \phi_{trig})/2\pi f \tag{2}$$

where U_c is some convective velocity with which the information of the changed wall condition is considered to advect. This effective fetch represents the virtual upstream position at which the flow encounters the step change. This model suggests that for the dynamically actuated surface, the mean velocity profile at some specific phase, will match the mean velocity profile of flow over a surface with a static spatial step change in roughness at a particular location upstream of the measurement location.

To test this hypothesis, measurements of the boundary layer were obtained over the device with a static step change in roughness. In Figure 6, the mean velocity profile for the step change at $\hat{x}/\delta \approx 2.1$ is shown by the dotted black lines for (*a*) rough-to-smooth case (R-S) and (*b*) smooth-to-rough case (S-R) along with the S0 and R0 profiles. They are seen to have the same behaviour as the transition profile for the F009 ($f = 2$Hz) case in Figure 3(*b*). For this case, if we assume $U_c/U_\infty = 0.18$, and set $\hat{x}_e = 2.1 \times \delta$ in Equation (2), we obtain $\phi_{obs} - \phi_{trig} = 0.22\pi$. The phase averaged profiles at $\phi = 0.22\pi$ and $\phi = 1.22\pi$ are also shown in Figure 6(*a*) and (*b*) respectively with open red symbols. The phase averaged profiles for the active cases at the matched effective fetch are seen to closely match the behaviour of the profiles of the static spatial heterogeneity cases.

To complete the model, we use Equation (2) with Equation (1) to obtain an expression for the IBL height, δ_i, as a function of phase which is given as:

$$\frac{\delta_i}{\delta} = A_0 \left(\frac{U_c(\phi_{obs} - \phi_{trig})}{2\pi f \delta} \right)^{\alpha} \tag{3}$$

In Figure 4, the computed IBL height, δ_i/δ as a function of phase is shown for the active cases by the red dashed line. For the value of $U_c \approx 0.18U_\infty$, we find that the computed front matches the shape of the front identified from the experimental data. The broad changes in the inclination of this front (in phase) with increasing f_δ are also well captured. However, this approach is based on empirical assumptions of the IBL growth rate and the power-law exponent can vary from $0.22 \leq \alpha \leq 0.86$, depending on the method used to define the IBL height (Rouhi *et al.*, 2019).

An alternative approach is to consider the diffusion analogy based model as proposed by Bou-Zeid *et al.*, 2004. In this approach, the IBL growth is considered to be proportional to the variance of the wall-normal velocity fluctuation (w_{rms}) and is given as $D\delta_i/Dt = Aw_{rms}$. Here, $D(.)/D(.)$ is the total derivative. By assuming $w_{rms} = CU_\tau$ (the downstream friction velocity), we obtain an expression for the IBL growth as a function of both time and fetch, as shown in Equation 4.

$$\frac{\partial \delta_i}{\partial t} + \frac{\partial \delta_i}{\partial x}\frac{\partial x}{\partial t} = CU_\tau \tag{4}$$

For the steady case, the time derivative term in Equation (4) is set to zero. Further, by setting $\partial x/\partial t = U(\delta_i)$, which can be evaluated by utilising an assumed form of the mean velocity profile (log + wake), Equation (4) can be numerically solved to obtain δ_i as a function of x, which can then be substituted for Equation (2), yielding an alternative form of Equation (3). The IBL front estimated with this method for $C = 0.9$ and $U_c/U_\infty = 0.18$ is shown in Figure 4 by the red cross marks. The front estimated with this method has excellent agreement with the front observed from the experiments for the range of non-dimensional frequencies studied here. An advantage of this method is that it is based on physical arguments and avoids the empirical power-law expression to predict the IBL growth.

Thus, based on the argument of an effective fetch, turbulent boundary-layer flows over an actively oscillating rough surface may be modelled as growing IBLs. The simplicity of the effective fetch argument allows the study of more applications of interest such as the case where the active roughness is in the form of streamwise travelling waves. If the wave velocity is denoted as c, and is defined to be positive along the flow direction, then the effective fetch is obtained by simply modifying the convection velocity term as $U_c - c$. The universality of the convection velocity term for a wider range of the dimensionless frequency as well as the strength of the perturbations at the wall (i.e. k_p of the roughness elements) remains to be studied.

Whilst this method of effective fetch seems to reasonably predict the flow response, it is not a true physical picture of the flow. In reality, the internal layer would develop simultaneously over the entire length of the installed roughness device. The information of the perturbation at the wall will propagate towards the free-stream, at some finite rate, at each streamwise position along the length of the installed surface as the internal layer is established. Additionally, the height from the wall to which the information travels increases as the fetch from the leading edge of the device increases. Thus, a challenge for future studies is to obtain a solution for Equation (4) that provides the IBL height as a function of both time and fetch.

CONCLUSIONS

Measurements of a turbulent boundary layer developing over an actively oscillating roughness with outer-scaled frequency $0.009 \leq f_\delta \leq 0.047$ are presented. For the lowest frequency case ($f_\delta \approx 0.009$), the phase averaged velocity profile is seen to oscillate between quasi-steady 'rough' and 'smooth' states, which match the static-smooth and static-rough limits of the roughness. The transition between the two states is identified as a forward leaning front in phase. As f_δ is increased, the transition state is seen to occupy a longer portion of the cycle. For $f_\delta \gtrapprox 0.018$, it is seen to extend beyond the half-cycle ($\phi = \pi$), where the wall condition changes. Beyond this dimensionless frequency, the outer part of the flow continues to develop for the previous wall condition even as the near-wall adapts to the new wall condition. Thus, $f_\delta \approx 0.018$ represents a critical frequency at which the mean velocity profile is perpetually in transition and no quasi-steady states are observed. It is also demonstrated that for quasi-steady phases during the dynamic cycle, the measured mean profile matches the profile observed for a static spatial step change from smooth-to-rough (or rough-to-smooth) at some streamwise fetch upstream of the measurement location. This suggests that flow over a surface with oscillating roughness can be modelled as a series of internal boundary layers (IBL). An effective fetch argument is proposed that relates the changing wall condition in phase to an equivalent streamwise position, based on a convective velocity, from which the IBL development can be modelled. When compared with static streamwise heterogeneous data at a known fetch, we find a good match at the predicted equivalent phase. The modelled fronts also match the fronts identified from the experiments. This strengthens the notion that turbulent boundary-layers developing over oscillating roughness can be modelled as internal boundary layers.

REFERENCES

Antonia, R.A. & Luxton, R.E. 1971 The response of a turbulent boundary layer to a step change in surface roughness. Part 1. Smooth to rough. *J. Fluid Mech.* **48** (4), 721–761.

Antonia, R.A. & Luxton, R.E. 1972 The response of a turbulent boundary layer to a step change in surface roughness. Part 2. Rough-to-smooth. *J. Fluid Mech.* **53** (4), 737–757.

Bou-Zeid, E., Meneveau, C. & Parlange, M.B. 2004 Large-eddy simulation of neutral atmospheric boundary layer flow over heterogeneous surfaces: Blending height and effective surface roughness. *Water Resour. Res.* **40** (2).

Chung, D., Hutchins, N., Schultz, M.P. & Flack, K.A. 2021 Predicting the drag of rough surfaces. *Annu. Rev. Fluid Mech.* **53**, 439–471.

Hartenberger, J.D., Callison, E.G., Gose, J.W., Perlin, M. & Ceccio, S.L. 2020 Drag production mechanisms of filamentous biofilms. *Biofouling* **36** (6), 736–752.

Hutchins, N. & Marusic, I. 2007 Evidence of very long meandering features in the logarithmic region of turbulent boundary layers. *J. Fluid Mech.* **579**, 1–28.

Jacobi, I. & McKeon, B.J. 2011 Dynamic roughness perturbation of a turbulent boundary layer. *J. Fluid Mech.* **688**, 258–296.

Li, M., de Silva, C.M., Chung, D., Pullin, D.I., Marusic, I. & Hutchins, N. 2021 Experimental study of a turbulent boundary layer with a rough-to-smooth change in surface conditions at high reynolds numbers. *J. Fluid Mech.* **923**.

Ligrani, P.M. & Bradshaw, P. 1987 Subminiature hot-wire sensors: development and use. *J. Phys. E: Sci. Instr.* **20** (3), 323.

Marusic, I. & Perry, A.E. 1995 A wall-wake model for the turbulence structure of boundary layers. Part 2. Further experimental support. *J. Fluid Mech.* **298**, 389–407.

Rouhi, A., Chung, D. & Hutchins, N. 2019 Direct numerical simulation of open-channel flow over smooth-to-rough and rough-to-smooth step changes. *J. Fluid Mech.* **866**, 450–486.

Stoodley, P., Lewandowski, Z., Boyle, J.D. & Lappin-Scott, H.M. 1998 Oscillation characteristics of biofilm streamers in turbulent flowing water as related to drag and pressure drop. *Biotechnol. Bioeng.* **57** (5), 536–544.

Talluru, K.M., Kulandaivelu, V., Hutchins, N. & Marusic, I. 2014 A calibration technique to correct sensor drift issues in hot-wire anemometry. *Meas. Sci. and Technol.* **25** (10), 105304.